

CHAPTER 3

Results and discussion

In this part, ZHS compounds were synthesized in surfactant-free solution by a microwave radiation. ZHS were produced from metal salts ($\text{SnCl}_4 \cdot 2\text{H}_2\text{O}$ and $\text{Zn}(\text{Ac})_2 \cdot 2\text{H}_2\text{O}$) in NaOH alkaline solution. They were synthesized at different pH solutions and microwave irradiation times. The final products were analyzed using XRD, XPS, FTIR, SEM, TEM, PL and UV spectroscopy. The results and discussion are shown the phases, atomic vibrations, morphologies, optical properties and compared the photocatalytic activity of ZHS which synthesized in different pH conditions and microwave irradiation times.

3.1 Structural and morphological characteristics

Figure 3.1 shows XRD patterns of the as-synthesized ZHS at different solution pH values by a microwave process. All the diffraction peaks of the typical samples can be indexed to the cubic $\text{ZnSn}(\text{OH})_6$ (JCPDS file No. 73-2384) with a cell edge of 7.8000 Å and space group of Pn-3 [83]. In this research, the pH is an important parameter to control the formation of ZHS phase and its crystalline degree. The sample synthesized at the pH 8 shows some weak and broad diffraction peaks, indicating that amorphous ZHS was synthesized. When the solution pH was increase to 11, a well-crystallized ZHS sample formed. Upon further increasing the solution pH from 11 to 14, the intensity peaks were slightly improved. The crystalline ZHS can be successfully synthesized at the pH > 11. The solution with a high concentration of OH^- promotes the formation of ZHS crystal.

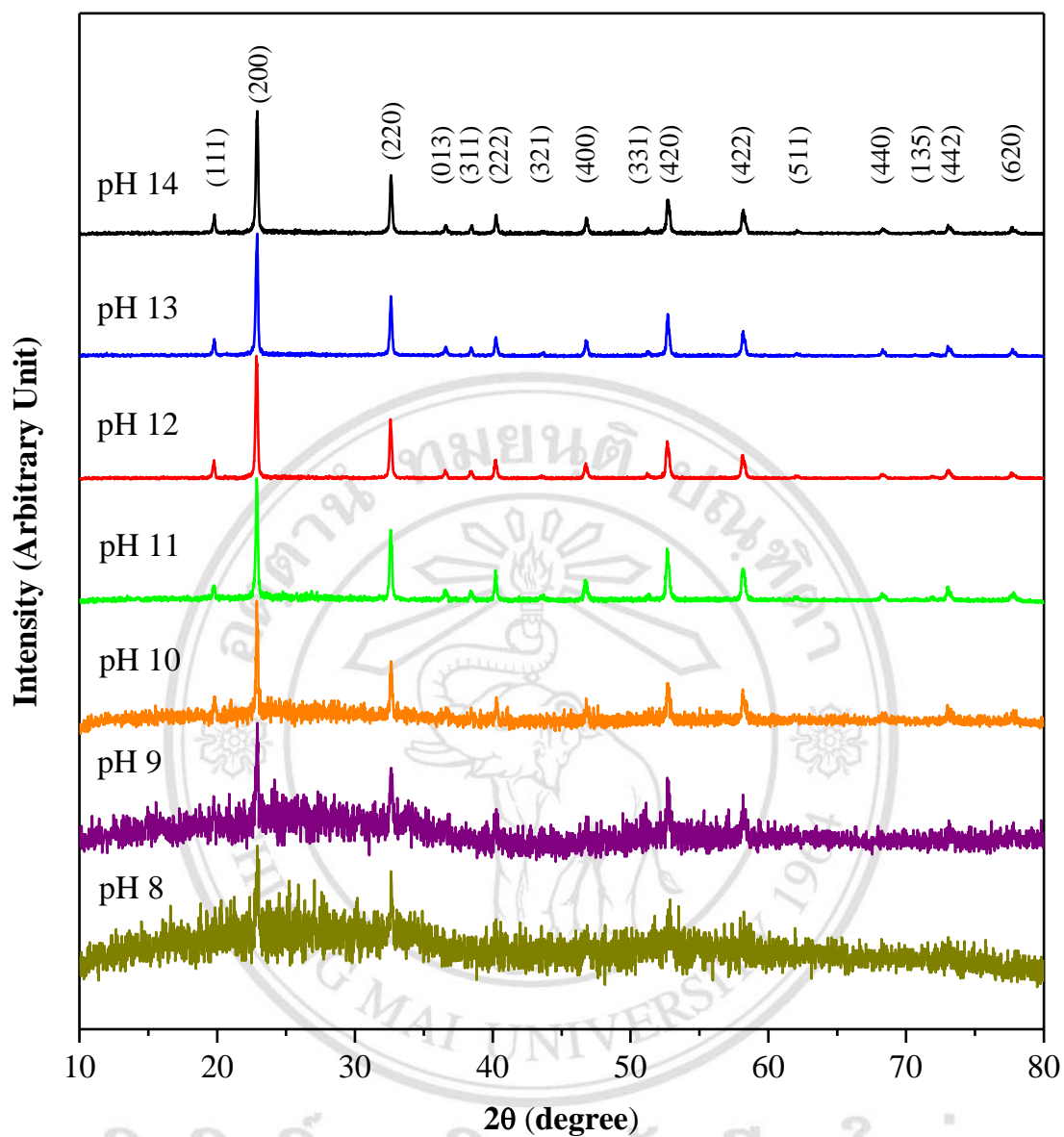


Figure 3.1 XRD patterns of cubic $\text{ZnSn}(\text{OH})_6$ synthesized in the solutions with the pH of 8 to 14 by a microwave method.

As shown in Figure 3.2, well-crystallized ZHS can be readily synthesized in a microwave irradiation range of 5–30 min. With further prolonging of the reaction to 30 min, the diffraction peaks of the ZHS become gradually stronger and narrower demonstrating the increase in crystallinity.

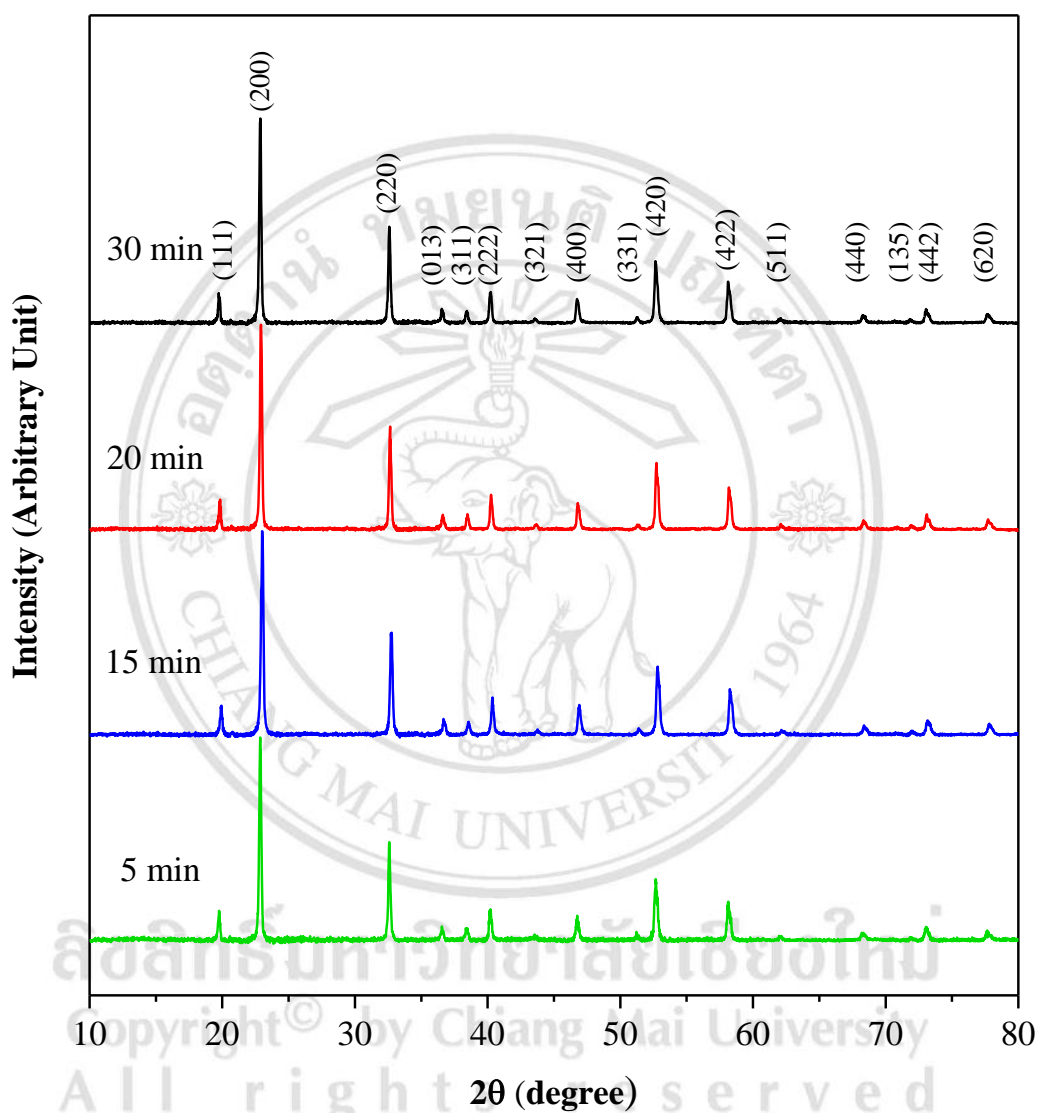


Figure 3.2 XRD patterns of the ZnSn(OH)₆ microcubes prepared at different times of microwave irradiation.

Furthermore, the crystallite size (D) on some specific lattice plane of ZHS was calculated by the Scherrer equation [23],

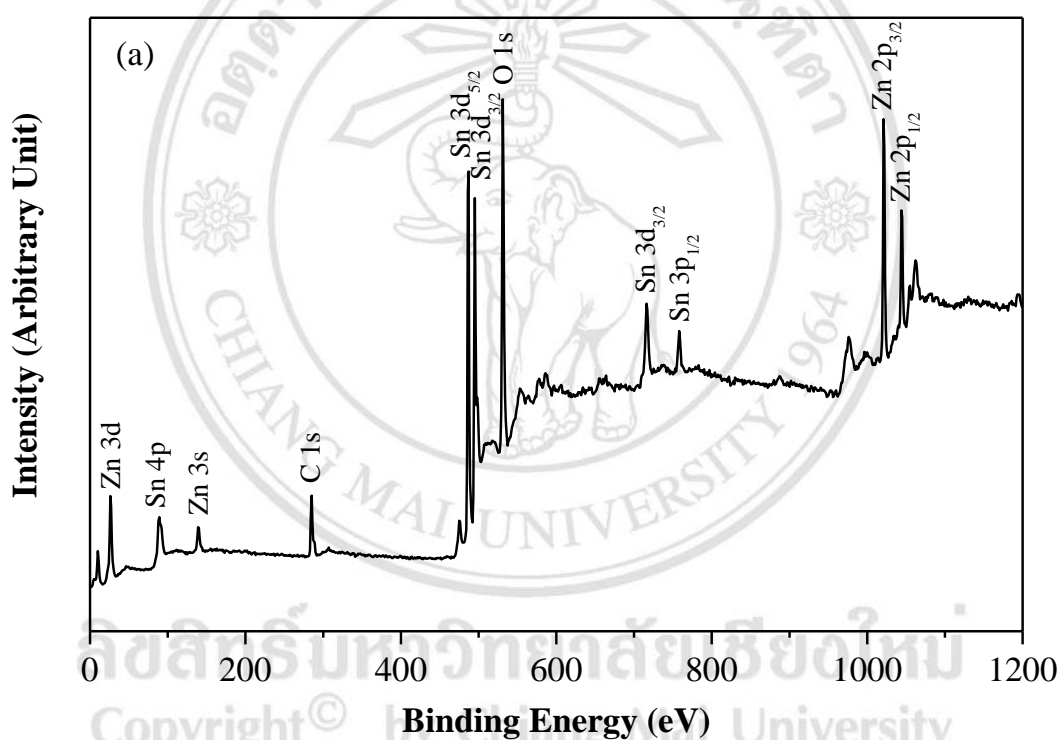
$$D = K\lambda/\beta \cos\theta \quad (3.1)$$

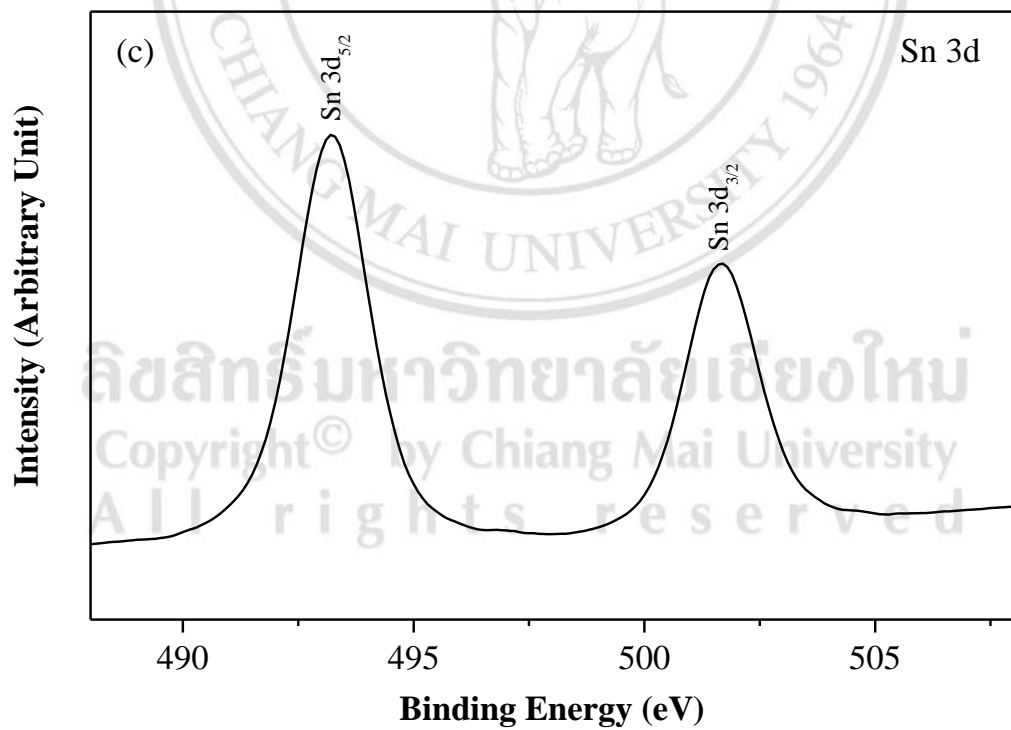
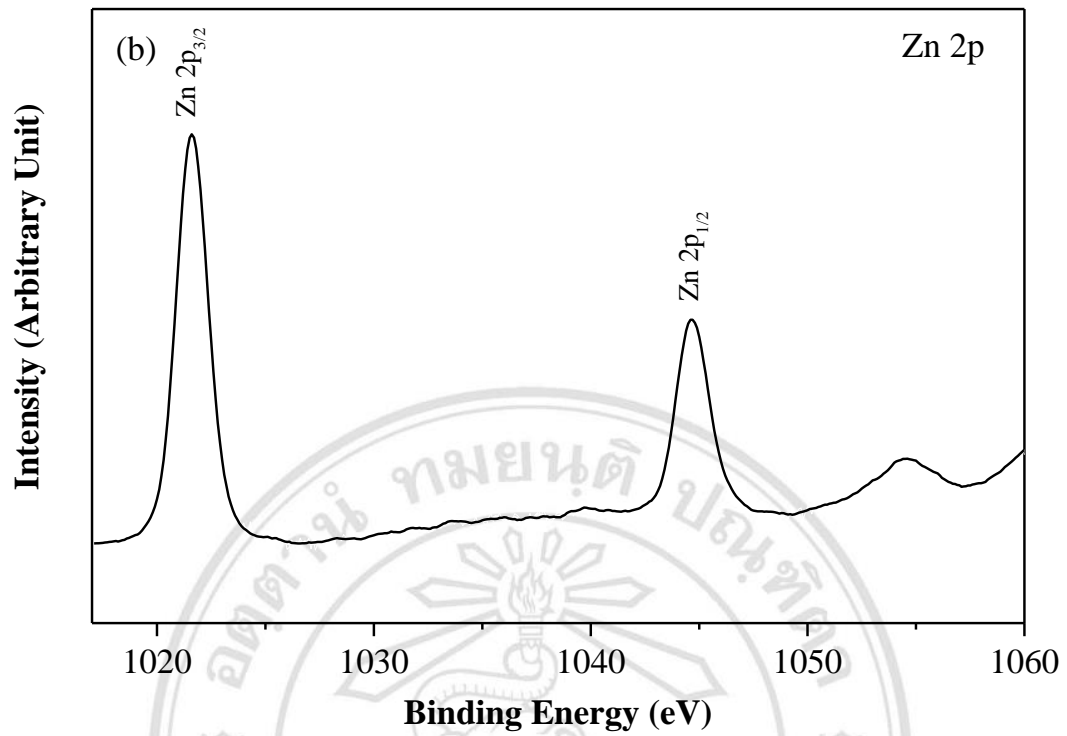
, where K is a constant (0.94), λ is the wavelength (Cu K_{α} = 0.15405 nm), θ is the Bragg angle and β is the full width at half maximum (FWHM) of a diffraction peak. According to Scherrer equation, the calculated crystallite sizes of these samples on plane (200) are given in Table 3.1, which are in the range of 42–46 nm.

Table 3.1 Crystallite size of ZHS prepared at different pH values.

Sample	Full width at half maximum; β (degree)	Diffraction angle; θ of (200) plane (degree)	Crystallite size (nm)
pH 11	0.1838	11.4388	46.4724
pH 12	0.1971	11.4313	42.9362
pH 13	0.1971	11.4388	42.0213
pH 14	0.1916	11.4463	44.1865

The chemical state and surface composition of the ZHS powders were characterized by X-ray photoemission spectroscopy (XPS) measurement. The full-scan spectrum in Figure 3.3a shows the presence of C, Zn, Sn, and O peaks, which confirmed the presence of these elements in the products. The carbon peak comes from the adventitious carbon on the surface of the sample. The Zn 2p consists of two peaks positioned at 1021.5 and 1044.6 eV for Zn 2p_{3/2} and Zn 2p_{1/2} (Figure 3.3b). The value correspond to the binding energy of Zn²⁺ ions. The peaks at 493.2 and 501.6 eV (Figure 3.3c) are assigned to Sn 3d_{3/2} and Sn 3d_{5/2} for Sn⁴⁺ state. The peak at 531.4 eV shown in Figure 3.3d corresponds to the binding energy of O 1s. These results revealed the successful synthesis of ZHS.





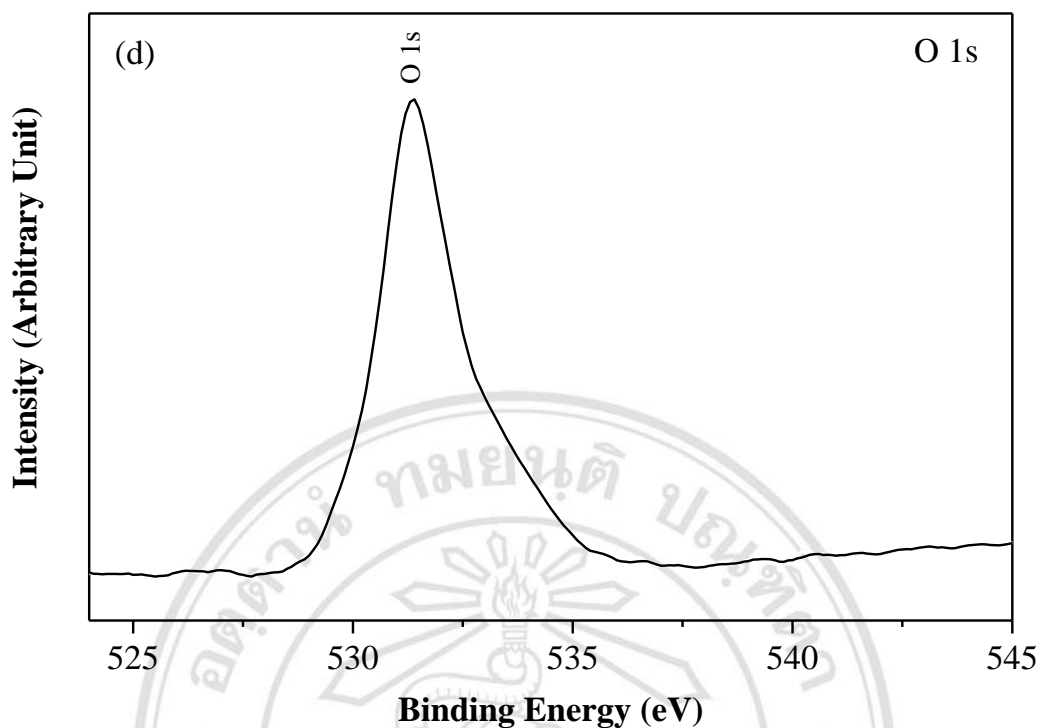


Figure 3.3 XPS spectra of $\text{ZnSn}(\text{OH})_6$ samples: (a) survey spectrum, (b) Zn 2p, (c) Sn 3d, and (d) O 1s.

The chemical structure of ZHS was characterized by FTIR, as the results shown in Figure 3.4. The band at 3200 cm^{-1} is assigned to OH stretching vibration, and the small band at 1632 cm^{-1} is ascribed to the OH bending vibration. The FTIR sharp band at 1175 cm^{-1} is caused by Sn–OH bending vibration. The band at 775 cm^{-1} is attributed to H_2O – H_2O hydrogen bonding. The band appeared at 540 cm^{-1} is assigned to the stretching vibration of Sn–O bonds [12, 29].

ลิขสิทธิ์มหาวิทยาลัยเชียงใหม่
Copyright © by Chiang Mai University
All rights reserved

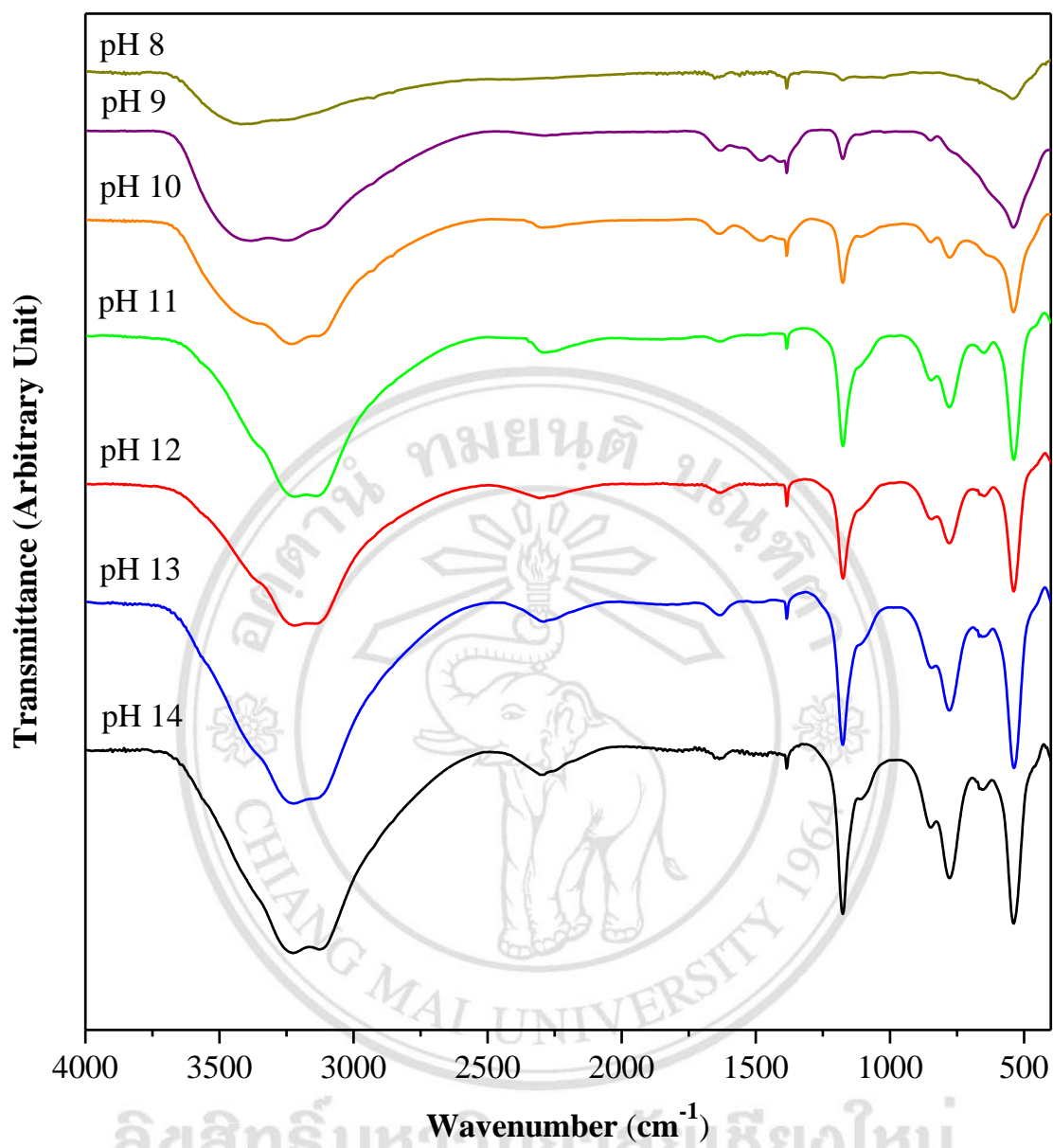


Figure 3.4 FTIR spectra of the cubic $\text{ZnSn}(\text{OH})_6$ synthesized at different pH solutions.

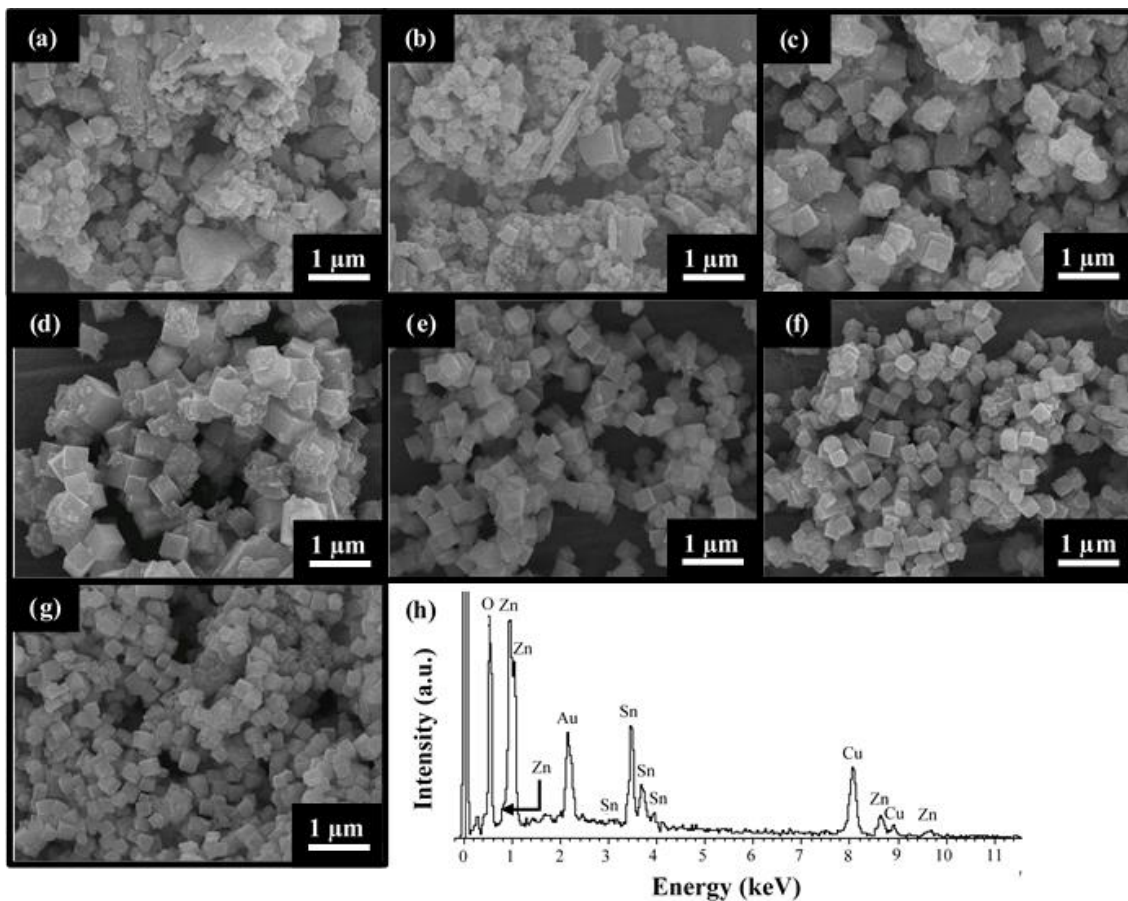


Figure 3.5 (a–g) SEM images of the cubic $\text{ZnSn}(\text{OH})_6$ synthesized by microwave irradiation at the pH of 8 to 14, respectively. (h) EDX spectrum of the cubic $\text{ZnSn}(\text{OH})_6$ synthesized at the pH of 14.

The morphology of ZHS samples synthesized at different pH conditions were characterized by SEM, as the results shown in Figure 3.5. SEM images of the samples clearly demonstrated the influence of alkalinity on morphology during the microwave-assisted synthesis of ZHS. The samples synthesized at the pH 8, 9 and 10 show no specific morphology. The hydroxide ions are not enough for the formation of regular particles. Upon increasing the pH to 11, homogeneous ZHS cubes with an average edge length of ~ 500 nm were mostly produced. Some nanoparticles attached on the surface of cubic crystals were detected, indicating that the as-obtained ZHS cubes were constituted by the oriented aggregation of tiny ZHS nanoparticles [19, 29]. At the pH 12–14, the ZHS products were entirely composed of large scale uniform monodispersive ZHS cubes. The average ZHS cubes are about 200 nm. The average size of microcubes remained

unchanged although the alkalinity was strengthened. The atomic constituents of as-synthesized ZHS cubic particles were determined by EDX and shown in Figure 3.5h. The EDX spectrum of ZHS cubic crystal revealed the presence of Zn, Sn and O with the Zn:Sn:O atomic ratio $\approx 1:1:6$, in accordance with the $\text{ZnSn}(\text{OH})_6$ chemical formula. Hydrogen atoms are too light to be detected by the present analysis. They should be noted that the sputtered Au for conductivity improvement and Cu stub for sample holder were also detected.

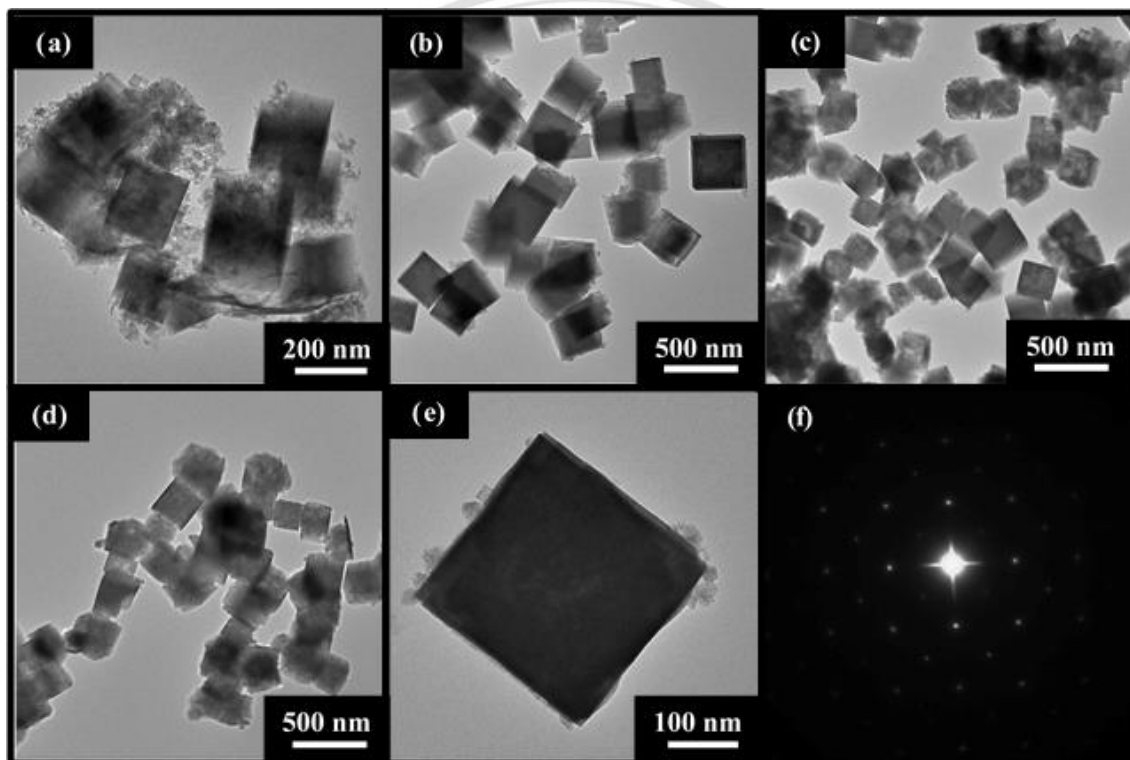


Figure 3.6 (a–d) TEM images of the $\text{ZnSn}(\text{OH})_6$ cubes obtained at the pH of 11 to 14, respectively. (e) High magnification TEM image and (f) SAED pattern of the individual $\text{ZnSn}(\text{OH})_6$ cube obtained at the pH of 14.

In addition, different morphologies of the as-grown ZHS cubes were characterized by TEM, as the results shown in Figure 3.6. The morphology displayed by the TEM images agrees well with those observed through the SEM. They should be noted that the surfaces of the as-obtained ZHS cubic crystallites are quite rough. They are composed of tiny ZHS nanoparticles with diameter of 10–50 nm, which validates the above SEM images. At the pH of 14, the sample was composed of a large number of boxes and the tiny nanoparticles

were no longer detected. The cubes were well dispersed without any aggregation. The TEM image of the free-standing ZHS cubic crystallite clearly shows that single microparticles has perfect cubic profile with very clear edges and corners. The corresponding selected area electron diffraction (SAED) pattern (Figure 3.6f) reveals the cubic crystalline structure of the ZHS single crystal. Thus, the SEM and TEM results suggest that the cubic ZHS formed by self-assembly of nanoparticles with the assistance of OH^- ions in the alkaline solutions.

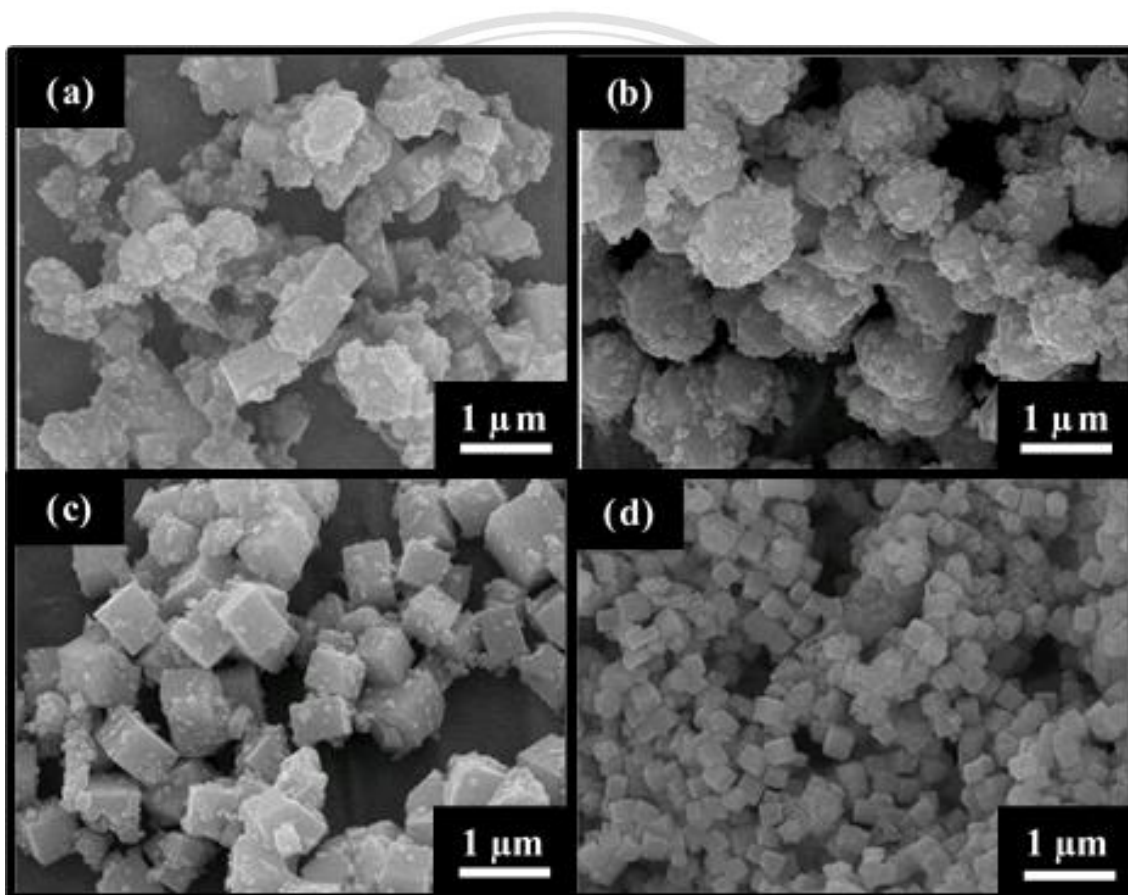


Figure 3.7 SEM images of morphology evolution of the $\text{ZnSn}(\text{OH})_6$ microcubes prepared at different lengths of microwave irradiation: (a) 5 min, (b) 15 min, (c) 20 min and (d) 30 min.

The time interval of microwave on the growth of the ZHS submicrocubes was also investigated, as the results shown in Figure 3.7. When the irradiation time was 5 min, a great number of irregular microparticles were synthesized. Upon increasing the irradiation time interval to 15 min, some non-uniform cubic particles appeared along with the irregular particles, indicating that the cube-like microparticles seemed to form

through the growth of irregular particles. When the irradiation time was lengthened to 20 min, the cubic structure became more evidence and appeared as non-uniform size of 500–600 nm. In order to obtain the perfect shape of cube structure, the irradiation time was lengthened to 30 min. The ZHS crystals obviously occurred conglomeration instead of becoming more perfect and regular. Based on the experimental results, a possible formation mechanism is proposed. First, ZHS was synthesized from metal salts ($\text{SnCl}_4 \cdot 2\text{H}_2\text{O}$ and $\text{Zn}(\text{CH}_3\text{COO})_2 \cdot 2\text{H}_2\text{O}$) in NaOH alkaline solution. Zn^{2+} and Sn^{4+} reacted with OH^- to form $\text{Zn}(\text{OH})_4^{2-}$ and $\text{Sn}(\text{OH})_6^{2-}$, which further combined and formed $\text{ZnSn}(\text{OH})_6$ by homogeneous/heterogeneous nucleation. Figure 3.8 shows the schematic of ZHS formation process and the chemical reaction equations can be explained as be by the following [84, 85].

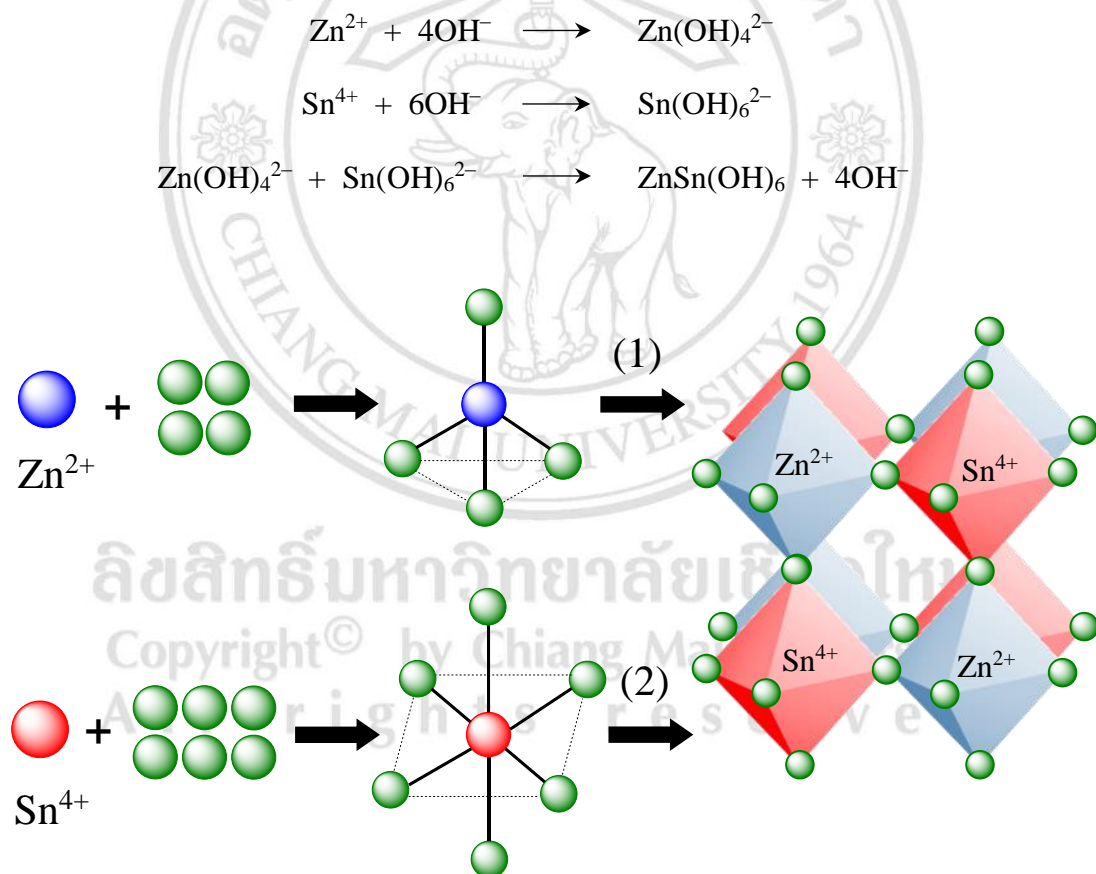


Figure 3.8 Schematic of $\text{ZnSn}(\text{OH})_6$ formation process.

According to Ostwald ripening law, ZHS precipitated and grew to form larger particles within a very short time under microwave. They aggregated to form cubic clusters with some nanoparticles attached on the surface of cubic crystal. Within a certain length of reaction time, the suspended nanoparticles were completely consumed, including that the perfect and uniform cubic crystallites were synthesized. The possible formation mechanism is schematically shown in Figure 3.9 [19, 85].

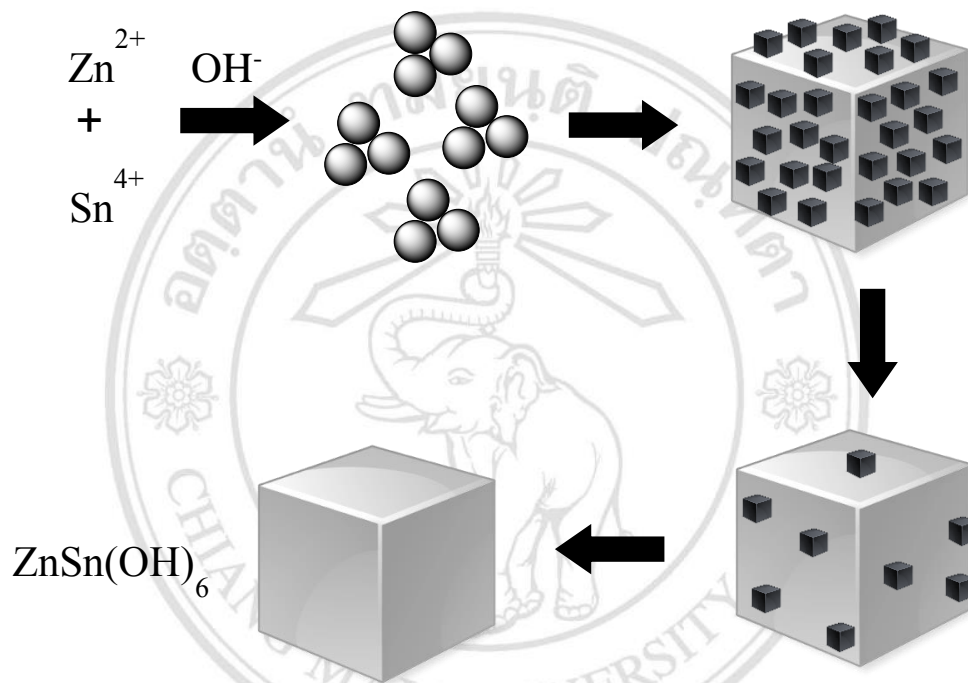


Figure 3.9 Schematic illustration of morphology evolution of the $\text{ZnSn}(\text{OH})_6$ microcubes prepared at different microwave radiation times.

ลิขสิทธิ์มหาวิทยาลัยเชียงใหม่
Copyright © by Chiang Mai University
All rights reserved

3.2 Surface area analysis

The specific surface area of the samples was obtained via a BET method. For the samples prepared at different pH, the area increases in sequence (11.34, 13.03, 13.18 and 13.69 $\text{m}^2\cdot\text{g}^{-1}$) as the basicity increases (pH of 11, 12, 13 and 14). The surface area of ZHS increases significantly with increase in the solution pH which is due to the increase in its average grain size. The variation of the morphology and specific surface area was caused by changing in the pH which can lead to influence the photocatalytic performance of the ZHS.

3.3 Optical characterization

Figure 3.10 shows UV–visible absorption of cubic–like ZHS synthesized under microwave. Electronic configurations of oxygen and tin are ${}^8\text{O}: 1s^2 2s^2 2p^4$ and ${}^{50}\text{Sn}: 1s^2 2s^2 2p^6 3s^2 3p^6 4s^2 3d^{10} 4p^6 5s^2 4d^{10} 5p^2$. The $5s^2$ and $5p^2$ are valence electrons of Sn and the $E(5s)$ is a little lower than the $E(5p)$. The shape spectrum exhibited absorption near UV region due to the electronic transition from O 2p to Sn 5s orbitals. The optical band gap of the ZHS cubes can be calculated according to the Tauc's formula by the following equation [79],

$$(\alpha h\nu)^n = B(h\nu - E_g) \quad (3.2)$$

, where α is an absorption coefficient, ν is a photonic frequency, h is the Planck's constant, B is a constant, and E_g is a band gap energy controlled by electronegativity, crystalline degree, defects and others. For ZHS direct semiconductor, n is equal to 2. The plot (Figure 3.11) indicates a gradual decreasing of absorbance attenuated through the ZHS solid. The absorbance was controlled by two photon energy ranges. For the photon energy $> E_g$, the absorbance was linearly increased with the increasing of photon energy. The inclination of the linear portion of the curve was caused by the absorption for charged diffusion from the highest occupied molecular orbital (HOMO) to the lowest unoccupied molecular orbital (LUMO). The energy difference between them is specified as the HOMO–LUMO gap characterized by a certain crystal momentum vector in the Brillouin zone, and is related to the spectral color. But for the photon energy $< E_g$, the absorbance became different from linearity, due to the absorption for charged diffusion relating to

defects. In general, the photoexcited electrons would recombine with the photogenerated holes by releasing energy as a photonic spectrum. When the momentum of electrons and holes is the same in both the conduction and valence bands, the electrons could directly emit a spectrum. In some cases, electrons must pass through an intermediate state and transfer momentum to the crystal lattice, and the electronic diffusion is related to an indirect energy gap. By extrapolating the linear portion curve to zero absorption, its direct energy gap was determined to be 3.68 eV. In this research, the cubes possess suitable electronic properties to cause redox reaction for the degradation of organic pollutants.

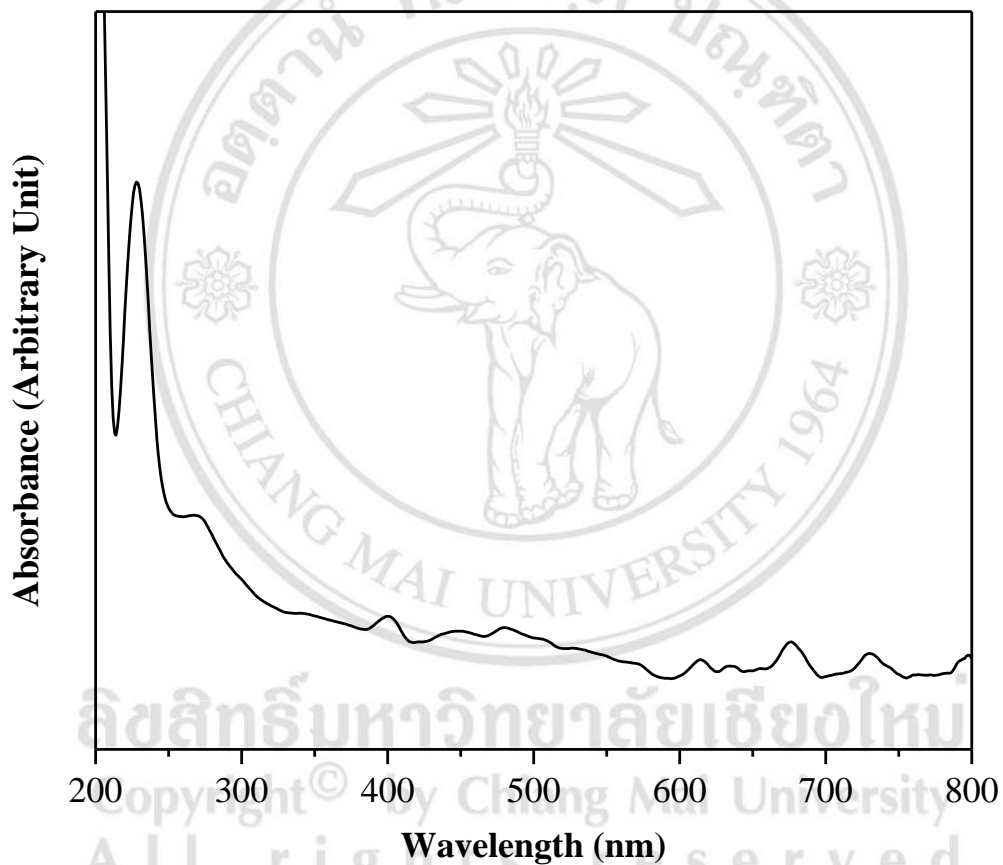


Figure 3.10 UV-visible absorption spectrum of cubic-like ZnSn(OH)₆ synthesized under microwave radiation.

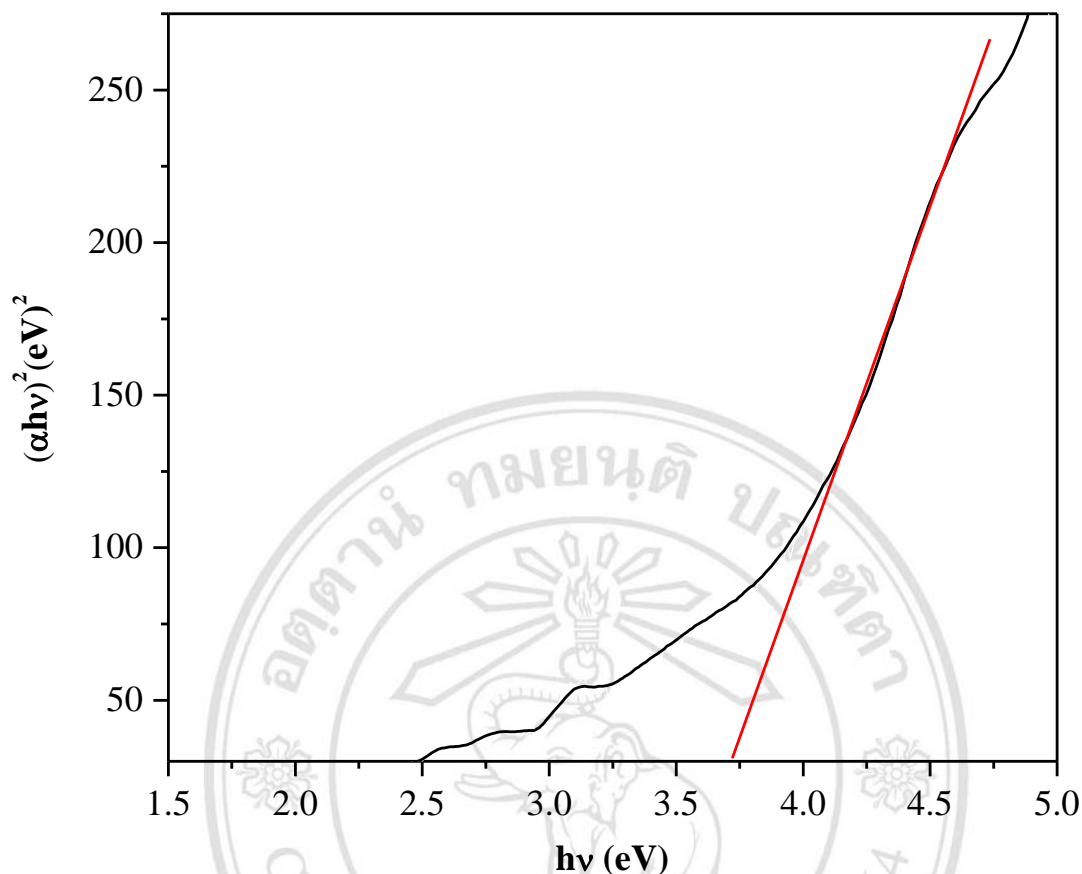


Figure 3.11 Plot of $(\alpha hv)^2$ versus $h\nu$ of cubic $ZnSn(OH)_6$ synthesized in the solution with the pH of 14.

The PL emission spectra have been used to study the separation efficiency of photogenerated charge carries in a semiconductor photocatalyst. The PL spectra of ZHS was measured at room temperature, as shown in Figure 3.12. The excitation wavelength is 280 nm. Two emission bands can be observed, which were centered at the 410 and 480 nm, respectively. The PL spectra features that two emission peaks centered at the 410 and 480 nm merged to form a broad band emission ranged from 350–600 nm. Similar results have been obtained by other investigation [30–31, 36]. In the previous investigations of the semiconductor nanomaterials the emission is often attributed to oxygen vacancies or to other kind of defects such tin vacancies O_2 interstitials. In addition, the ZHS microcubes with high surface should also favor the existence of large quantities of oxygen vacancies. These oxygen vacancies induce the formation of new energy levels in the band gap of ZHS. The recombination of a photo-excited hole with an electron occupying an oxygen vacancy yields the emission.

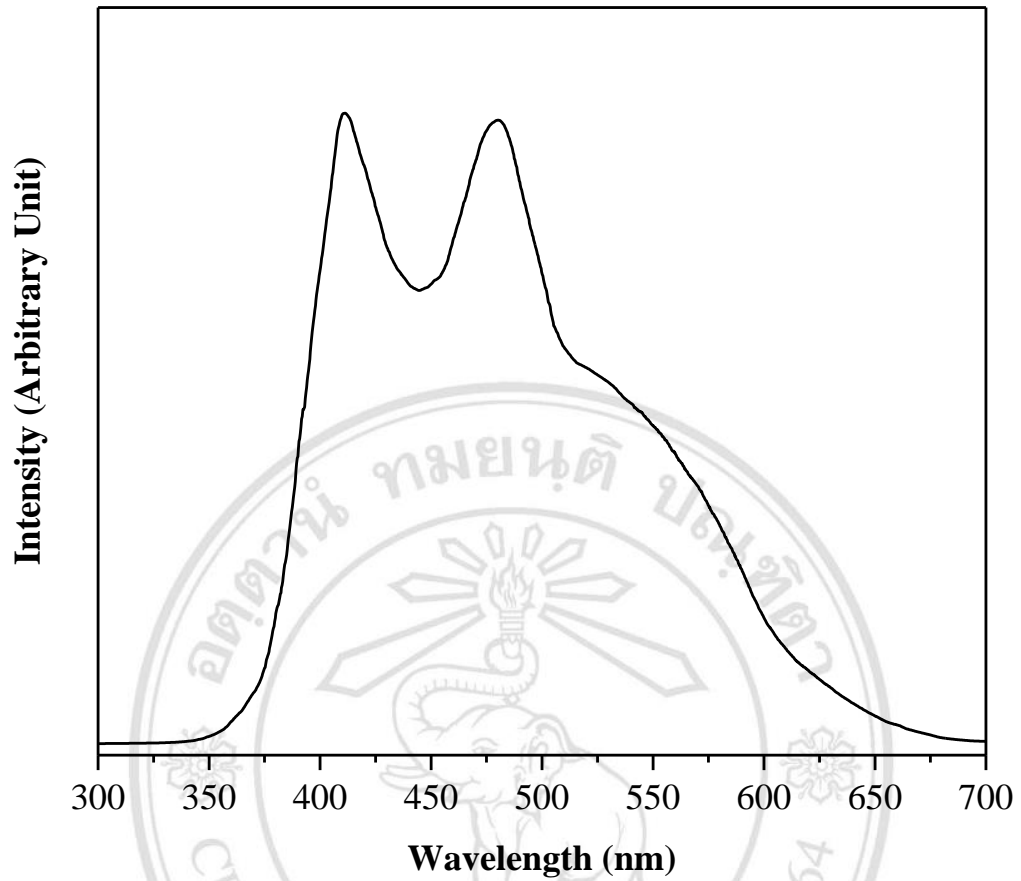


Figure 3.12 PL spectra of ZnSn(OH)₆ microstructure. The excitation wavelength is 280 nm.

ลิขสิทธิ์มหาวิทยาลัยเชียงใหม่
Copyright© by Chiang Mai University
All rights reserved

3.4 Photocatalytic activity

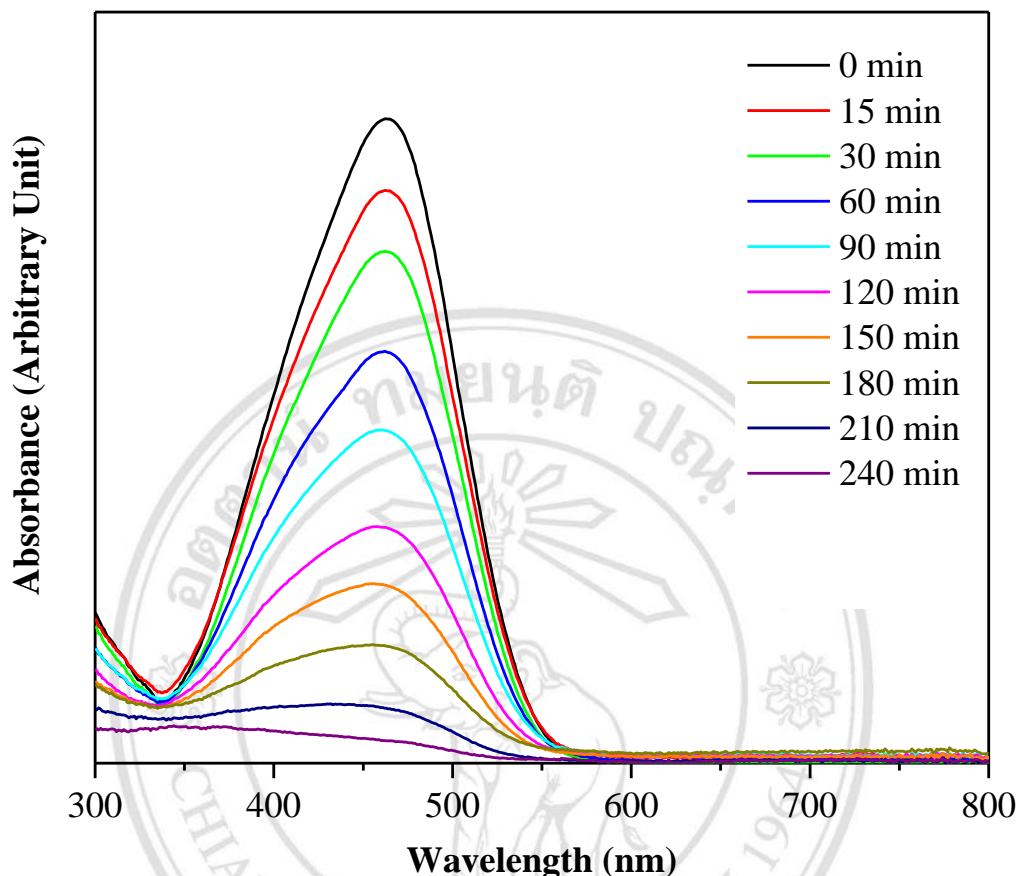


Figure 3.13 UV–visible absorption of methyl orange (MO) dye in the solution containing ZnSn(OH)_6 (synthesized in the solution with the pH of 14) irradiated by UV radiation for different lengths of time.

The cubic-like ZHS with the best crystal was used for photocatalytic test. The photocatalytic activities of the ZHS synthesized at the pH of 11, 12, 13 and 14 were measured through the degradation of MO solutions under UV light irradiation. Figure 3.13 shows the temporal evolution of absorbance during the photocatalytic degradation of MO in the solution containing ZHS. The absorption peak at 463 nm corresponding to the MO molecules decreases in intensity rapidly with the length of illumination time. The position of absorption peaks shows hypsochromic shifts because of the deethylated degradation process in a stepwise manner. The ZHS has good degradation rate for the MO dye, which is completely degraded within 240 min.

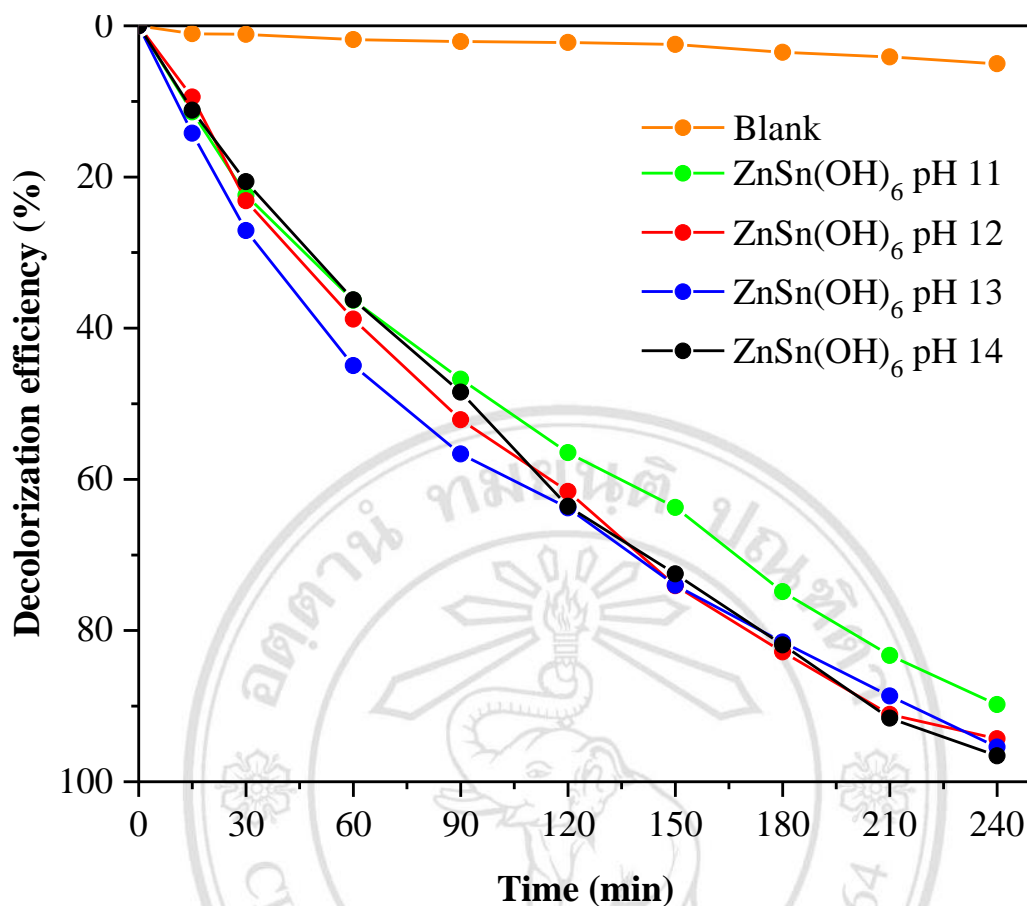


Figure 3.14 Decolorization efficiency of methyl orange (MO) dye solutions containing ZnSn(OH)₆ photocatalyst synthesized in the solution with the pH of 11 to 14, comparing with that of the blank under UV radiation.

Figure 3.14 shows the photocatalytic performance of the ZHS samples synthesized in the solutions with the pH of 11–14 and the blank test without the catalyst. A negligible photodegradation of MO was observed in the absence of the photocatalyst. Within 240 min irradiation, MO dye decolorized and the decolorization efficiency of MO were listed in Table 3.2.

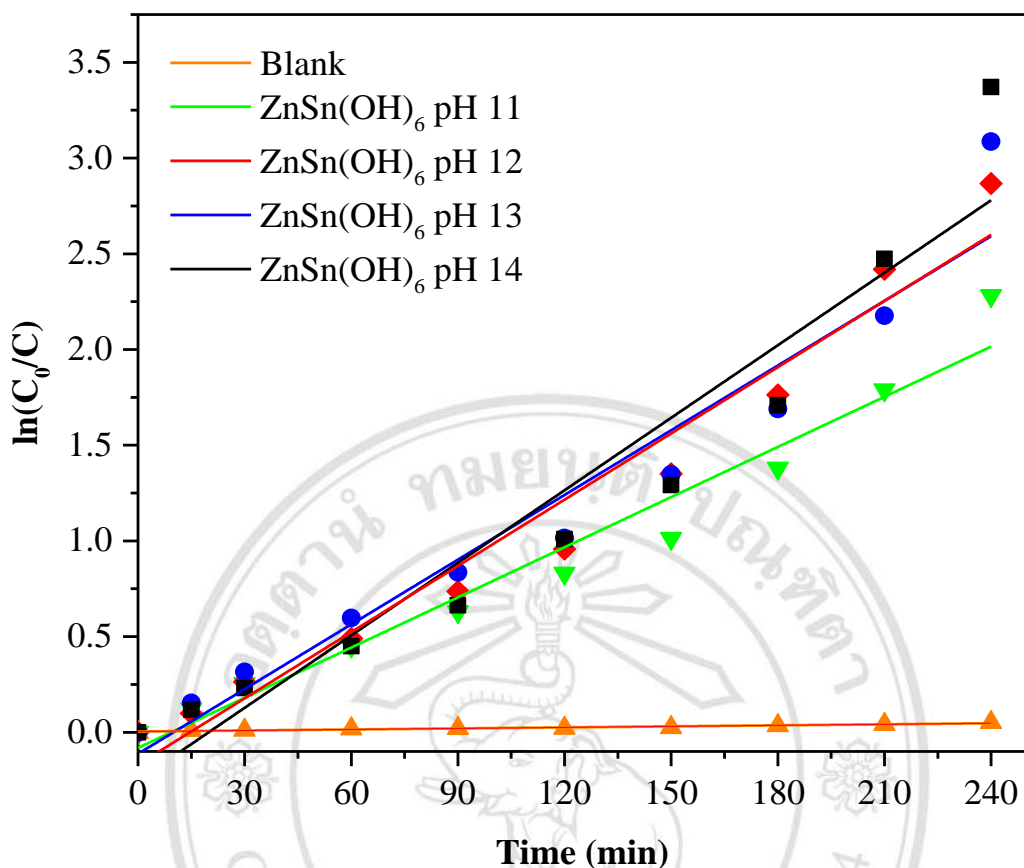


Figure 3.15 First-order reaction kinetic plots of the photodegradation of methyl orange (MO) dye solutions containing ZnSn(OH)₆ photocatalyst synthesized in the solutions with the pH of 11 to 14, comparing with that of the blank under UV radiation.

The degradation rate can be described using the first-order kinetic equation expressed as follows

$$\ln(C_0/C) = kt \quad (3.3)$$

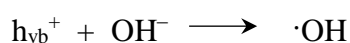
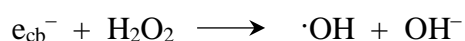
, where C_0 is the initial concentration of the MO solution, C is the MO concentration with in the irradiation time (t) and the slope k is the apparent reaction rate constant [86]. The reaction rate for MO degradation photocatalyzed by the samples is shown in Figure 3.15, corresponding to the linear relationship between $\ln(C_0/C)$ and the irradiation time. The estimate apparent degradation rate constants of ZHS synthesized in the solutions with the pH of 11 to 14 were calculated and listed in Table 3.2. In contrast, the k rate constant of the blank was only 0.0002 min^{-1} . Comparing among the different photocatalysts of the

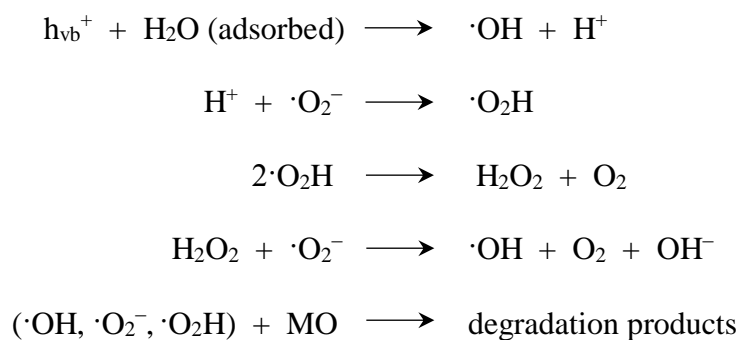
present research, the cubic-like ZHS synthesized in the solution with the pH of 14 displayed the highest rate constant. In general, the photocatalytic performance is strongly controlled by morphology and surface area of the materials. The ZHS sample with the largest BET surface area exhibited the highest MO photodegradation efficiency.

Table 3.2 The results of photocatalyst measurement of synthesized samples.

Sample	Surface Area $\text{m}^2\cdot\text{g}^{-1}$	% Decolorization	Rate constant (k ; min^{-1})
pH 11	11.34	89.79	0.0087
pH 12	13.03	94.31	0.0115
pH 13	13.18	95.43	0.0113
pH 14	13.69	96.56	0.0126

In aqueous solution, the photocatalytic degradation of the dye is caused by the active species produced on the surface of semiconductors. When the photocatalyst is illuminated by UV light with photon energy higher than the band gap of the semiconductor, electrons in the valence band can be excited to the conduction band of the photocatalyst and reacted with adsorbed oxygen molecules to form superoxide anion radicals ($\cdot\text{O}_2^-$). Concurrently, photogenerated holes were left in valence band, reacting with the adsorbed $\text{H}_2\text{O}/\text{OH}^-$ on the surface of the photocatalyst to form hydroxyl radicals ($\cdot\text{OH}$). The obtained radicals are strong oxidizing agents, and are able to oxidize most of azo dyes to the mineralization end-products. The photocatalytic reaction can be expressed by the following [26, 27].





ZHS is a class of perovskite-structured hydroxide and contains hydroxyl groups as part of its lattice [11]. The OH^- on ZHS can play an important role in the photocatalysis. The OH^- species accept photogenerated holes to form $\cdot\text{OH}$ radicals which are very active in photocatalytic reaction. $\cdot\text{OH}$ is generally derived through the oxidation of adsorbed H_2O by h_{vb}^+ . The hydroxyl group on ZHS supplies large quantities of M-OH ($\text{M} = \text{Sn}$ or Zn) and consequently facilitates this formation. The surface OH^- is consumed during the photocatalytic process. Thus, the regeneration of surface OH^- is the important precursors to sustain $\cdot\text{OH}$ radicals. The adsorption of H_2O and the subsequent regeneration of OH^- ions are favorable to provide photocatalysis.

Moreover, the stability and reusability of the ZHS photocatalyst were further evaluated by repeating experiment on the degradation of MO under UV radiation, as the results presented in Figure 3.16 Even after five cycles, 90 % of MO was degraded by the re-used ZHS. The photocatalytic rate constants of the ZHS for the 1st to 5th cycle were about 0.0115, 0.0113, 0.0106, 0.0105 and 0.0095 min^{-1} , respectively (Figure 3.17). The high photoactivity of the re-used ZHS remains unchanged within 20 h.

Copyright© by Chiang Mai University
All rights reserved

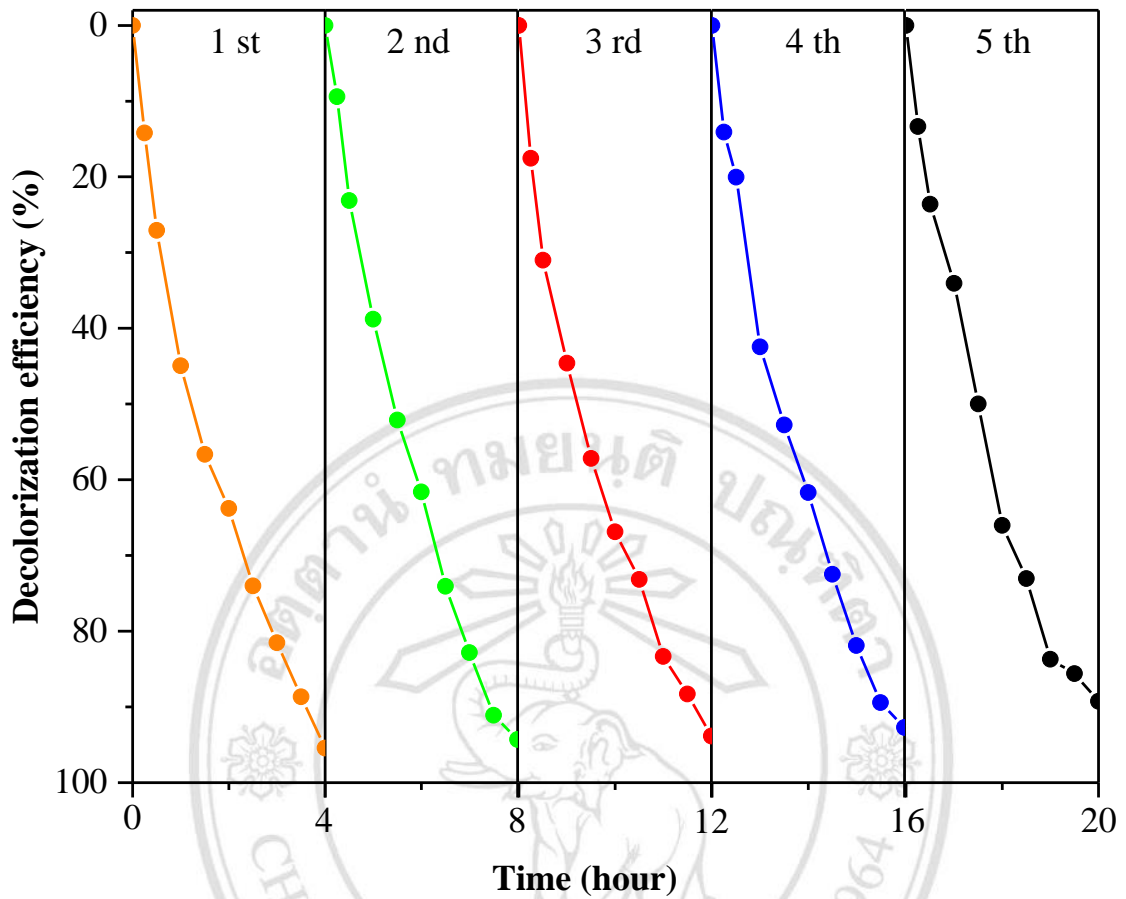


Figure 3.16 Recyclability for the photodegradation of methyl orange (MO) dye solution by $ZnSn(OH)_6$ photocatalyst (synthesized in the solution with the pH of 14) under UV radiation up to five cycles.

ลิขสิทธิ์มหาวิทยาลัยเชียงใหม่
 Copyright© by Chiang Mai University
 All rights reserved

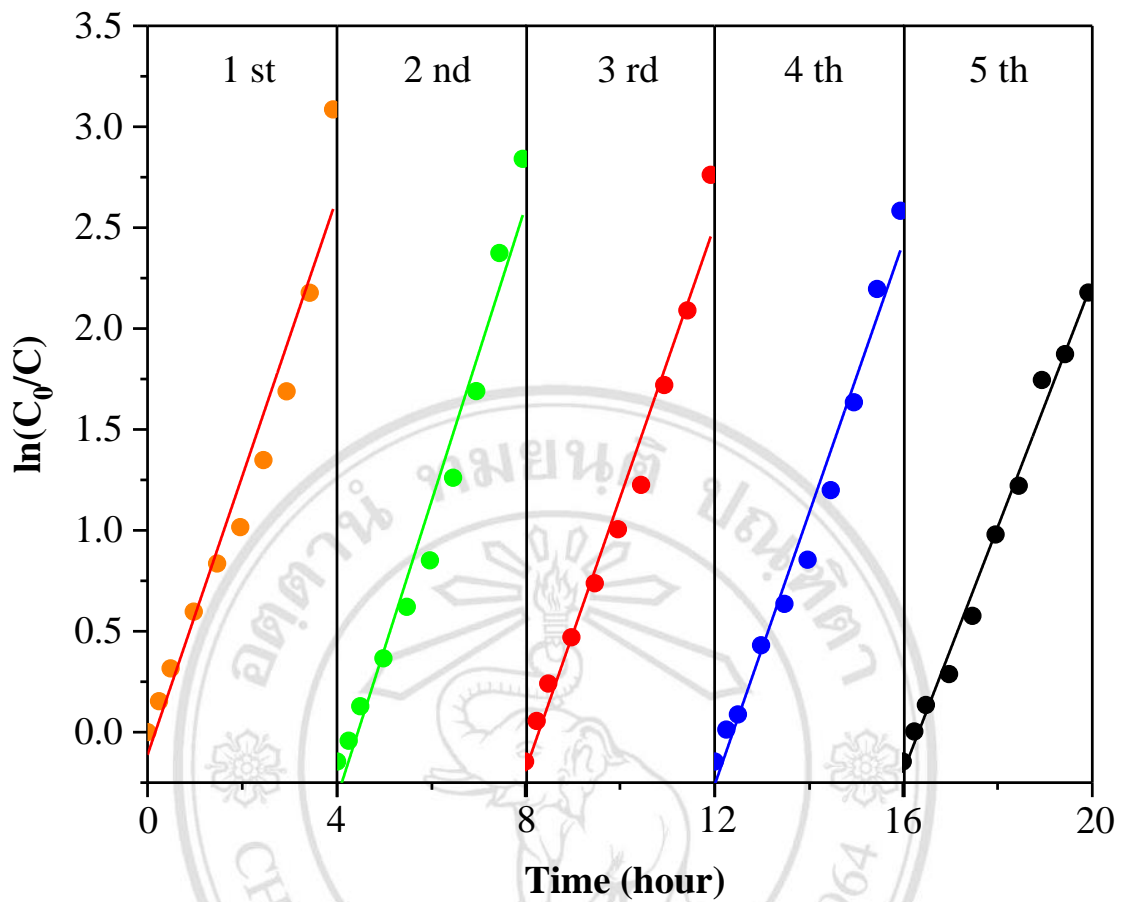
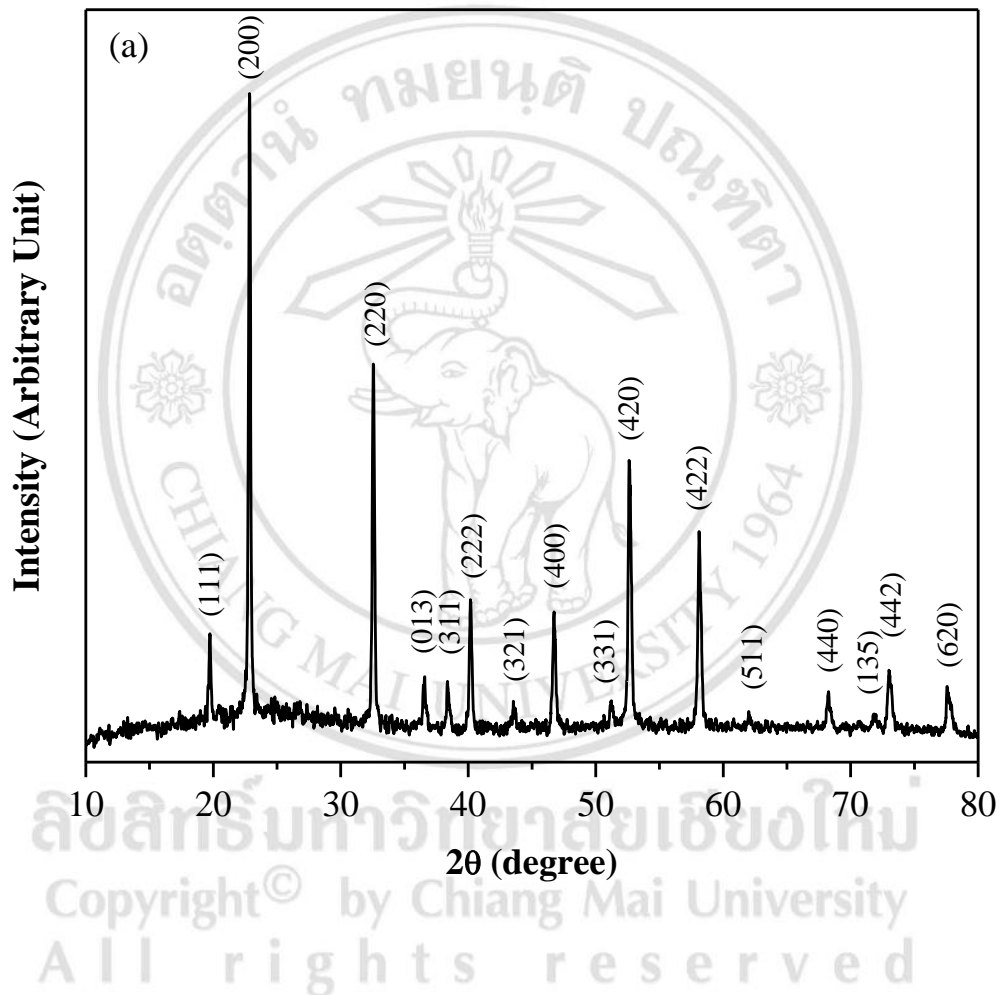


Figure 3.17 Pseudo first order kinetics of ZnSn(OH)₆ photocatalyst for repeated degradation of methyl orange (MO) dye up to five cycles.

ลิขสิทธิ์มหาวิทยาลัยเชียงใหม่
 Copyright© by Chiang Mai University
 All rights reserved

Further XRD and FTIR analyses of the re-used ZHS photocatalyst after five-cycle run are presented in Figure 3.18. The diffraction peaks are still corresponding to ZHS (JCPDS file No. 73-2384) without any change in their intensity suggesting the structural intact [83]. In contrast, FTIR spectrum of the used ZHS exhibits no obvious change as compared to that before photocatalytic testing. The evidence confirms that the ZHS photocatalyst is stable and is not degraded during the photocatalytic oxidation of MO molecules.



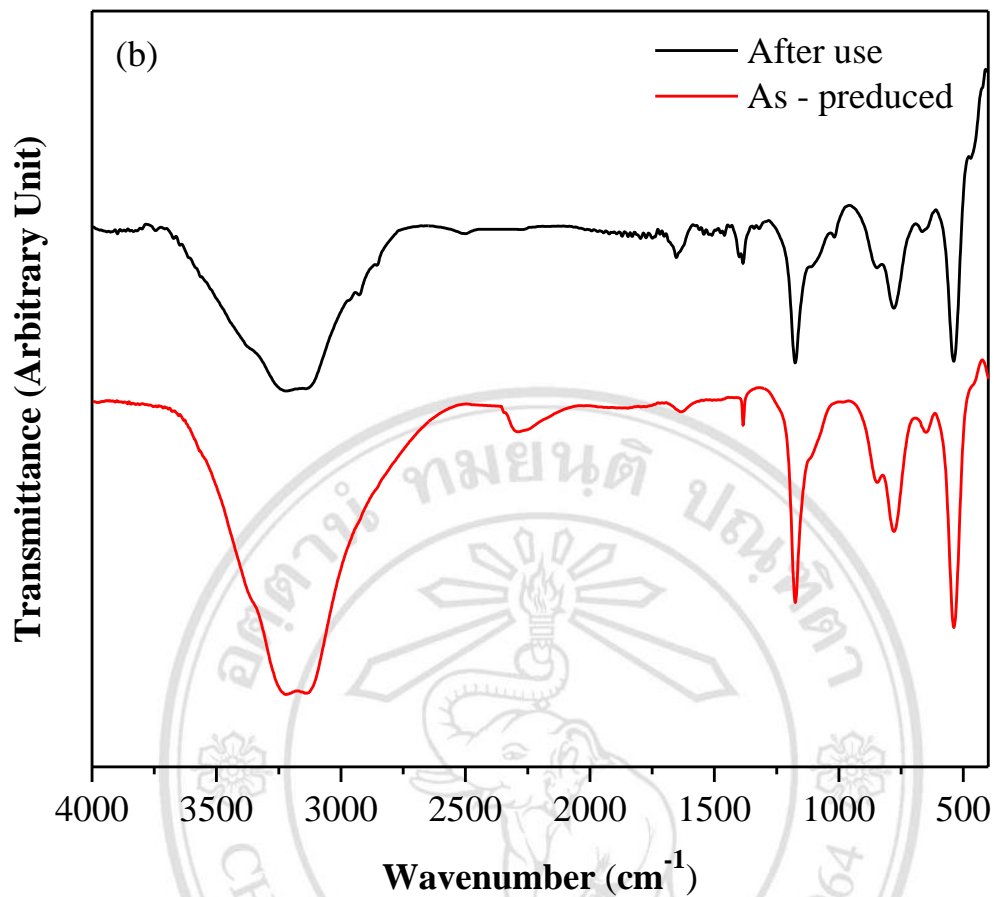


Figure 3.18 (a) XRD pattern of the recovered $\text{ZnSn}(\text{OH})_6$ after five cycle testing, and
(b) FTIR spectra of the as-synthesized and recovered $\text{ZnSn}(\text{OH})_6$ samples.

ลิขสิทธิ์มหาวิทยาลัยเชียงใหม่
Copyright© by Chiang Mai University
All rights reserved